Bulletin of the Seismological Society of America, Vol. 98, No. 6, pp. 2948–2961, December 2008, doi: 10.1785/0120060252

High-Resolution Seismic Images and Seismic Velocities of the San Andreas Fault Zone at Burro Flats, Southern California

by C. C. Tsai,* R. D. Catchings, M. R. Goldman, M. J. Rymer, P. Schnurle, and H. W. Chen

Abstract To better understand the structure of the San Andreas fault (SAF) at Burro Flats in southern California, we acquired a three-dimensional combined set of seismic reflection and refraction profiles centered on the main active trace at Burro Flats. In this article, we discuss the variation in shallow-depth velocities along each seismic profile, with special emphasis on the 1500 m/sec *P*-wave velocity contour, which can be an indicator of shallow-depth water-saturated unconsolidated sediments. Along the four seismic profiles, minimum depths of the groundwater table, as inferred from 1500 m/sec velocity contour, range from 10 to about 20 m. The largest variations in depth to the top of the groundwater table occur in areas near mapped faults, suggesting that the groundwater flow in Burro Flats is strongly affected by the locations of fault traces. We also used the seismic data to develop seismic reflection images that show multiple strands of the SAF in the upper 60 m. Reflectors above the 10 m depth probably correspond to Holocene alluvial deposits; reflectors below the 15 m depth probably arise from velocity or density variations within the Precambrian gneiss complex, likely due to weathering. Apparent vertical offsets of reflectors are observed along profiles (lines 1 and 2) that are normal to the SAF, indicating minor apparent vertical offsets on the SAF at shallow depths. Along line 2, the apparently vertically offset reflectors correlate with zones of relatively low *P*-wave velocity. Along the central part of lines 1 and 2, the faults form a flower structure, which is typical of strike-slip faults such as the SAF.

Introduction

Burro Flats is a small basin bounded on the southwest by the San Andreas fault (SAF) within the San Bernardino Mountains and immediately north of the San Gorgonio Pass, about 140 km east of Los Angeles, California (Fig. 1). Understanding the earthquake hazards associated with the SAF in the San Gorgonio Pass area is important because of nearby population centers and because multiple major lifelines to the larger population centers in southern California trend through the San Gorgonio Pass. Paleoseismological investigations suggest that the southern SAF has produced approximately 14 large earthquakes within the past 1500 yr (Fumal *et al.*, 2002). Recent studies of the structurally complex SAF at the Burro Flats site indicate that five distinct events occurred at approximately A.D. 1500–1850, 1400–1550, 1300–1450, 700–1100, and 450–800, suggesting recurrence intervals between 100 and 475 yr and an average recurrence interval of about 300 yr (Yule and Sieh, 2001). Given that the last event is believed to have been between A.D. 1500 and 1850 and that the average recurrence interval is about 300 yr, the area may be currently due for another large event. However, to fully understand the slip history of Burro Flats, it is important to first determine the fault geometry at Burro Flats to assess if other strands of the fault have been recently active. For this purpose, we acquired combined seismic reflection and refraction data in the vicinity of the mapped main trace designed to (1) image auxiliary strands in the shallow subsurface and (2) measure shallow subsurface velocities associated with fault strands.

Geologic and Tectonic Setting

The SAF is highly complex in the vicinity of the San Gorgonio Pass, where it forms a contractional left step (Matti *et al.*, 1985; Matti and Morton, 1993) and the surface trace disaggregates into a knot of irregular and discontinuous faults (Allen, 1957; Matti and Morton, 1993; Yule and Sieh, 2001) (Fig. 1). Southeast of the San Gorgonio Pass, the SAF splits into two segments: the Mission Creek segment, which extends north of the San Gorgonio Pass within the San Bernardino Mountains and the Banning segment, which trends largely along the southern end of the San Bernardino Mountains. The Banning segment of the San Andreas fault may be

*Current address: Institute of Oceanography, National Taiwan University, P.O. Box 23-13, Taipei, Taiwan 106.

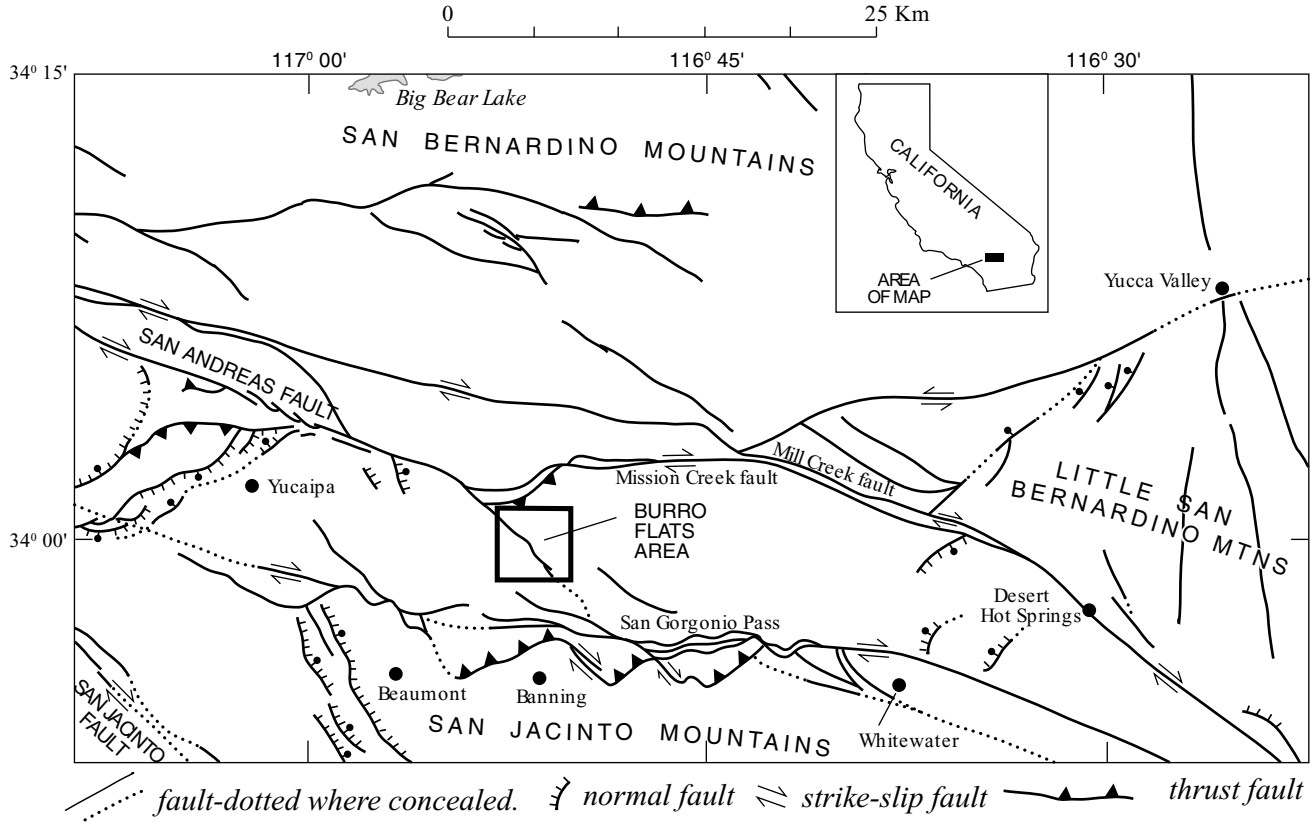

Figure 1. Fault map of the San Gorgonio Pass region (from Rymer [2000]). Box shows regional location of the study area.

up to 100 km in length and has generated as much as 16–25 km of right-lateral slip since the late Miocene (Matti *et al.*, 1985). In the San Gorgonio Pass area, however, the Banning fault has been modified by Quaternary reverse, thrust, and wrench faults, the assemblage of which is called the San Gorgonio Pass fault zone. Right-lateral movement apparently continues near the southern end of the Banning fault and was the source of the 1986 *M* 5.9 North Palm Springs earthquake (Jones *et al.*, 1986; Sharp *et al.*, 1986; Nicholson, 1996), but the westernmost segment of the Banning fault may be inactive, as there is little evidence of ground rupture during the Quaternary (Matti *et al.*, 1985).

The San Gorgonio Pass is covered by Quaternary sediments that include Holocene and Pleistocene alluvial fan deposits and Holocene active channels and washes (Matti *et al.*, 1985). Lithologies within the San Bernardino Mountains to the north and the San Jacinto Mountains to the south consist largely of metamorphic rocks that have been intruded by plutonic rocks of quartz monzonitic composition (Matti *et al.*, 1985). The intrusive dikes include pegmatite dikes, migmatitic rocks (granitic composition), and plutonic quartz monzonite rocks. Allen (1957) describes these rocks as a hybrid of types of varying composition and transitional boundaries that resulted from complex faulting within the San Bernardino Mountains. To the south, the crystalline rocks of the San Jacinto Mountains are largely Mesozoic, Paleozoic, and Precambrian granitoid and prebatholithic metasedimentary rocks (Matti *et al.*, 1985), consisting largely of quartzo-feldspathic gneisses and schists, hornblende schists, phyllite, crystalline limestone, and quartzite (Fraser, 1931). The metasedimentary rocks are underlain by intrusive rocks that are predominantly of granodiorite composition (Allen, 1957).

Burro Flats is located within a structurally complex part of the SAF zone in the San Bernardino Mountains, north of the San Gorgonio Pass (Fig. 2a). At Burro Flats, the SAF consists of a series of straight right-lateral-segment stepovers, separated by pull-apart basins. In the southeastern part of Burro Flats and southward, the SAF is relatively straight and less complex. In the northwestern part, the fault zone consists of at least two fault strands (blue lines in Fig. 2b). The two main fault strands strike northwest–southeast along the axis of a synform: a linear northeast strand and an arcuate southwest strand. The northeast strand may offset the contact between younger and older alluvial fan deposits by as much as 50 m (Yule *et al.*, 2001). The southwest strand cuts the southwest limb of the synform and shows a consistent upon-the-south component of offset (Yule *et al.*, 2001). The Burro Flats trench site, located about 8 km north of Banning, lies within a marsh that formed within a 75 m wide pull-apart basin between right-stepping traces of the San Bernardino strand of the SAF (Fig. 2b). Recent excavation at Burro Flats indicates that the SAF dips 75° southwest in the near surface (Yule *et al.*, 2001). Paleoseismological trenches expose the

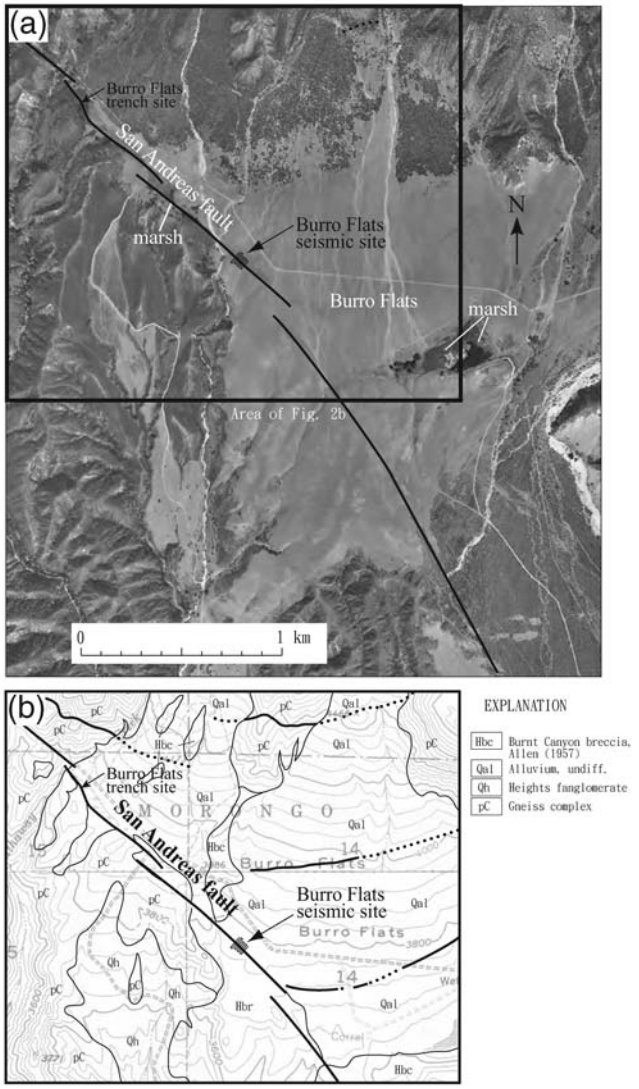

Figure 2. Location of the study area. (a) Aerial photo of Burro Flats area, with the San Andreas fault shown in red and the location of the seismic investigation. Paleoseismic trench sites by Yule *et al.* (2001) are shown in yellow north of the seismic imaging site. The box outlined in black shows the location of Figure 2b. (b) Geologic map of the study area (from Yule *et al.* [2001]). The site of the Burro Flats seismic investigation is shown in red. Mapped strands of the San Andreas fault are shown in blue. Trench sites by Yule *et al.* (2001) are shown northwest of the seismic investigation site.

southwestern edge of the step-over basin, where the primary basin-bounding fault juxtaposes poorly sorted, older, very coarse gravel against interbedded peat, sand, and coarse gravel. North- and south-facing scarps are locally preserved in Holocene alluvium. Short north-striking faults (Riedel shears) splay off of the main fault zone into the marsh (Fig. 2a; Yule *et al.*, 2001; Yule and Sieh, 2003). Yule *et al.* (2001) indicate these faults to be right-lateral normal oblique faults that transfer slip across the pull-apart basin. Other structural features, including fissures and folds, are within the area between the southwestern boundary fault and the transfer faults, with the exception of a broad open fold that occurs farther east in the marsh.

Data Acquisition

We acquired combined high-resolution seismic reflection and refraction data centered on the main surface trace of the SAF at Burro Flats (Fig. 2b). The seismic investigation included a 300 m long seismic profile across the main active trace and a 60×70 m rectangular array centered on the main trace. In this article, we only present data and results from the rectangular array. Seismic data were acquired along receiver lines using a shoot-through acquisition technique, whereby the recording sensors remained stationary as shots were fired through the recording arrays. To present two-dimensional (2D) cross sections across the array, we extracted lines 1, 2, 3, and 4 from the seismic data set of the rectangular array (Fig. 3).

Approximately 3 sec of data were recorded on two Geometrics Strataview™ RX 60 seismographs, each with 60 active channels. Seismic sources and sensors (geophones) were colocated (1 m separation) and spaced at 5 m increments on the northeast–southwest-trending lines (lines 1 and 2) and at 10 m increments on the northwest–southeast-trending lines (lines 3 and 4). We used a combination of 0.45 kg explosions in 1 m deep boreholes and 400 grain Betsy–Seisgun™ blanks in 0.3 m deep holes to generate the seismic sources. Sensors consisted of 40 Hz single-element Mark Products L-40A™ vertical geophones. We used up-hole times to determine timing for the explosions and electronic triggers for the Betsy–Seisgun blasts. Data were recorded without acquisition filters at a sampling rate of 0.5 msec. Representative shot gathers from each of the four profiles are shown in Figure 4. Because of relatively low cultural noise in the area, signal-to-noise ratios were high, and most sources were sufficient to propagate across the entire array.

Seismic Data Processing

Because we acquired the seismic data using a shoot-through method, we were able to develop both refraction (velocity) and variable-fold reflection images from the same data. The combined reflection and refraction data provide strong constraints on the composition and structures of the shallow subsurface. Below, we describe the 2D processing methods for the refraction and reflection data, and we present the resulting velocity models and reflection images.

Seismic Refraction Velocity Analysis

First-arrival refractions from seismograms were used to develop a *P*-wave tomographic velocity model of the shallow subsurface along each seismic profile. To measure first-arrival refractions, we band-pass filtered the data between 50 and 400 Hz (Fig. 4). We used a modified version of an algorithm by Hole (1992) to invert the first arrivals for the

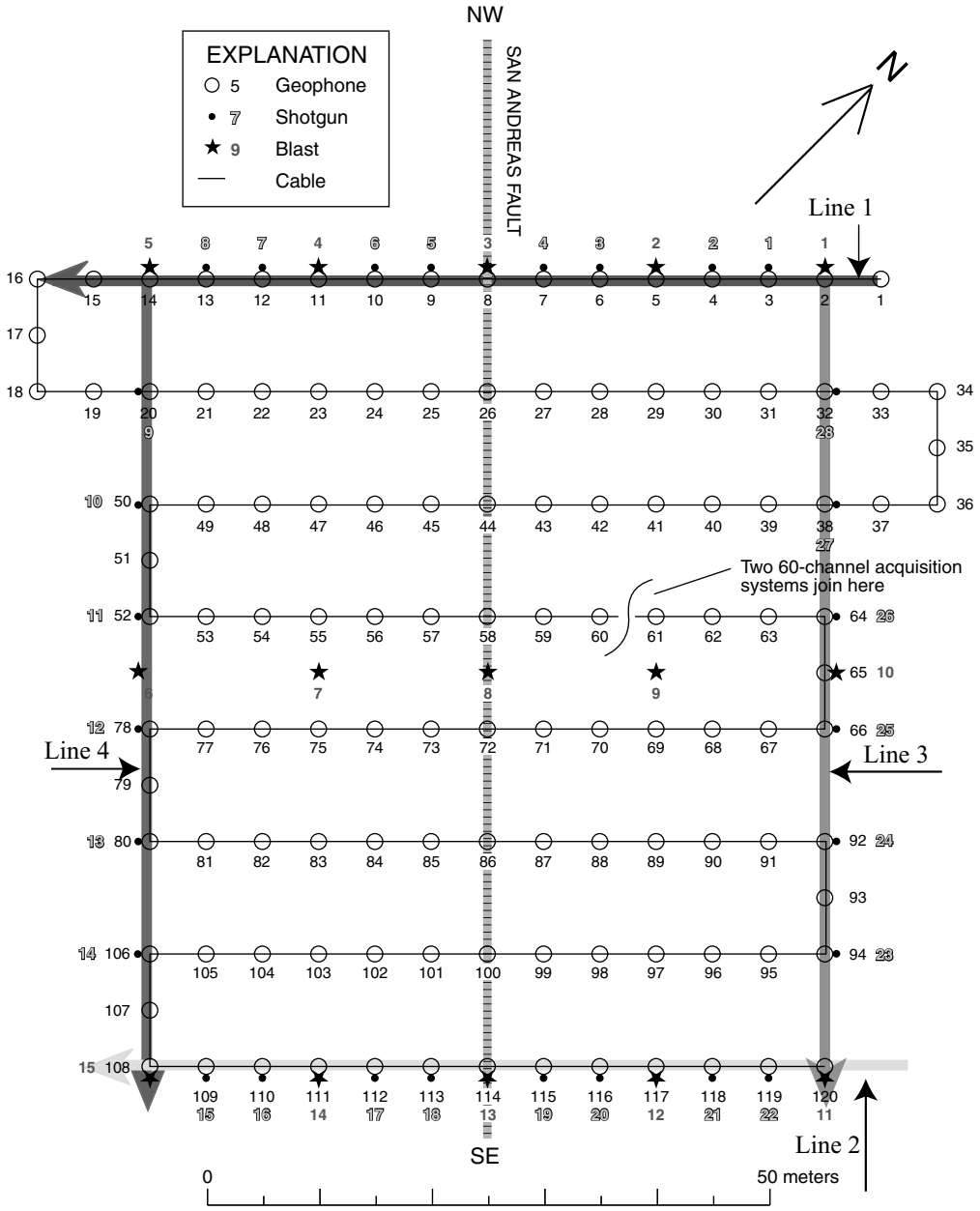

Figure 3. The geometrical setup of the seismic investigation at Burro Flats. The locations of shots, consisting of explosions (stars) and shotgun blasts (dots), and the locations of geophones (open circles) are shown. Each shot was recorded by all receivers (geophones). The seismic investigation includes a 60×70 m rectangular array. Lines 1, 2, 3, and 4 are shown in color and are discussed in this article. The northwestern projection of the mapped trace of the San Andreas fault is shown as the dashed line.

velocity structure. In developing the tomographic velocity model, we used several different starting models, but the final models converged to similar final models. In general, the velocity models are best resolved in the upper 50% depth range of the models, where the density of the ray coverage is the highest. We smoothed the model both vertically and horizontally over three grid cells (3×3 m). Thus, the vertical and horizontal resolution of our study approaches 5 m^2, where the ray coverage is sufficiently dense. The minimum depth of the velocity image is related to the length of the lines and the shot (5 m) and geophone (5 m) spacing. The maximum depth of the velocity image was limited by the maximum offset where clear first arrivals could be measured on the shot gathers. Velocity imaging ranged in depth between about 1 m below the surface to maximum depths of about 35 m. For greater depths, velocities needed for seismic reflection stacking were determined using semblance and parabolic methods. Within the depth range of the tomographic velocity

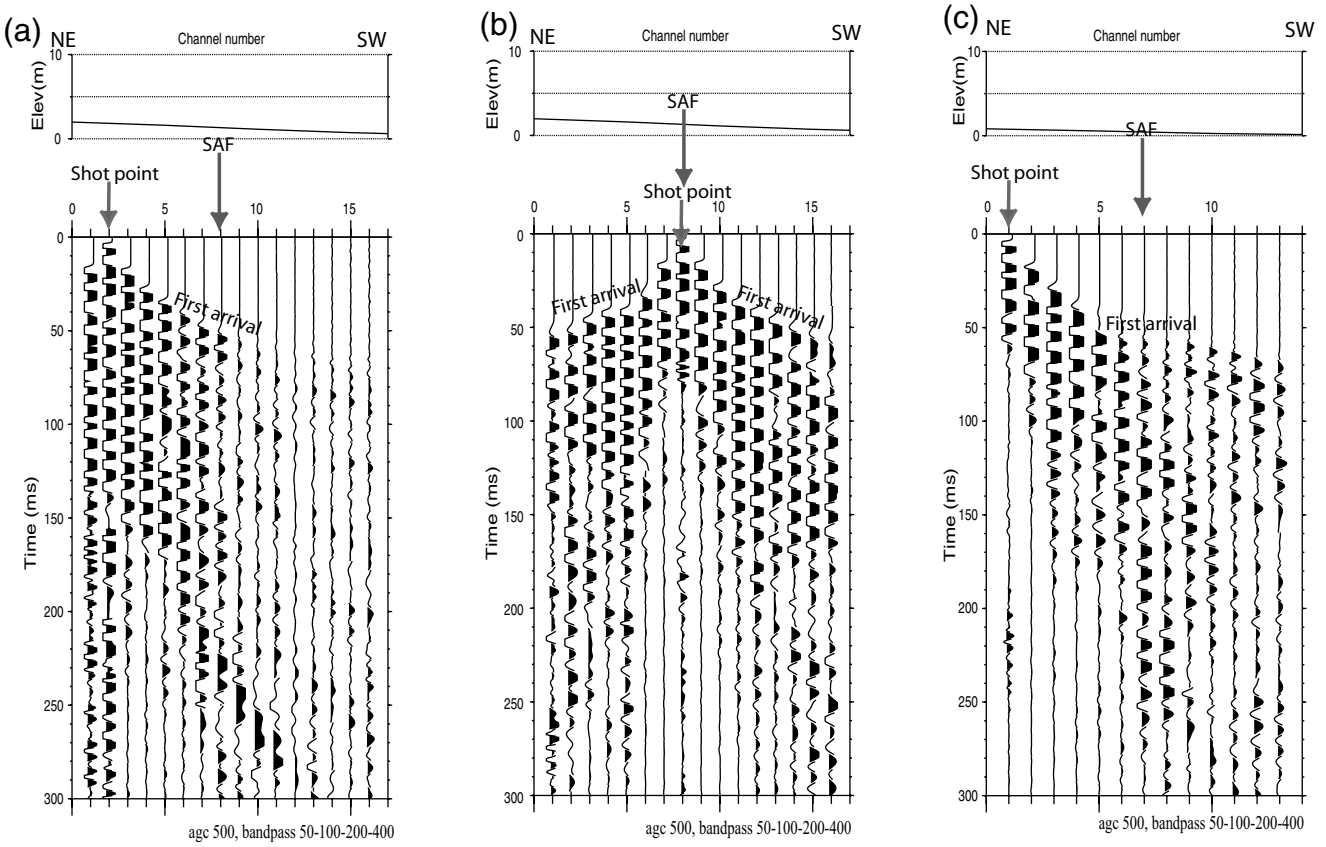

Figure 4. Representative shot gathers from each seismic line. The horizontal axis shows the channel number and the vertical axis shows travel time in milliseconds. Shot points are shown by the blue arrow; the mapped trace of the location of the San Andreas fault is shown by the red arrow (along lines 1 and 2). Elevation along the line is shown above the shot gathers. The data were band-pass filtered between 50 and 400 Hz. (a) A shot gather with the shot point located near the northeastern end of line 1. (b) Shot gather with the shot point located near the central part of line 1. (c) Shot gather with the shot point located near the northwestern end of line 2. (d) Shot gather with the shot point located near the central part of line 2, plotted as in Figure 4a. (e) Shot gather with the shot point located near the southeastern end of line 3. (f) Shot gather with the shot point located near the southeastern end of line 4. (*Continued*)

model, we used the inversion-derived velocities to convert the reflection time images to depth images and to migrate the seismic reflection images.

Reflection Data Processing

For seismic reflection data processing, we used procedures similar to those outlined by Brouwer and Helbig (1998). The following steps were involved in data processing: geometry installation, trace editing, timing corrections, elevation statics, top muting, bottom muting, band-pass filtering, velocity analysis, and Kirchoff prestack depth migration.

Seismic Image Interpretations

Seismic velocity and reflection images were developed along each of the four intersecting lines from the surface to maximum depths of about 35 m. Line 1 trends northeast–southwest, nearly perpendicular to the surface trace of the SAF (Fig. 3). Migrated seismic reflection images of the upper 100 m of line 1 are shown in Figure 5a. These data are reflective from the near surface to depths of approximately 65 m; however, most of the reflectors are not continuous across the seismic profile. Migrated images show subhorizontal strata with slightly northeastward dips in the upper 50 m along most of line 1. Although there are lateral variations, there are principal changes in reflectivity at depths of about 10, 20, and 60 m, which are probably related to differences in lithology and/or physical properties of subsurface rocks at those depths.

Line 1 Refraction Section

Compressional-wave velocities range from about 400 m/sec at the surface to about 3500 m/sec at about 25 m in depth (Fig. 5). In the San Gorgonio Pass region, detailed seismic refraction measurements and well logs show that sediments with velocities of about 1500 m/sec correspond to the depth of the static water level (Catchings *et al.*, 1999; Gandhok *et al.*, 1999). Based on the known lithology of Burro Flats (Yule *et al.*, 2001) and our measured velocities, we interpret the stata with velocities less than 1500 m/sec to

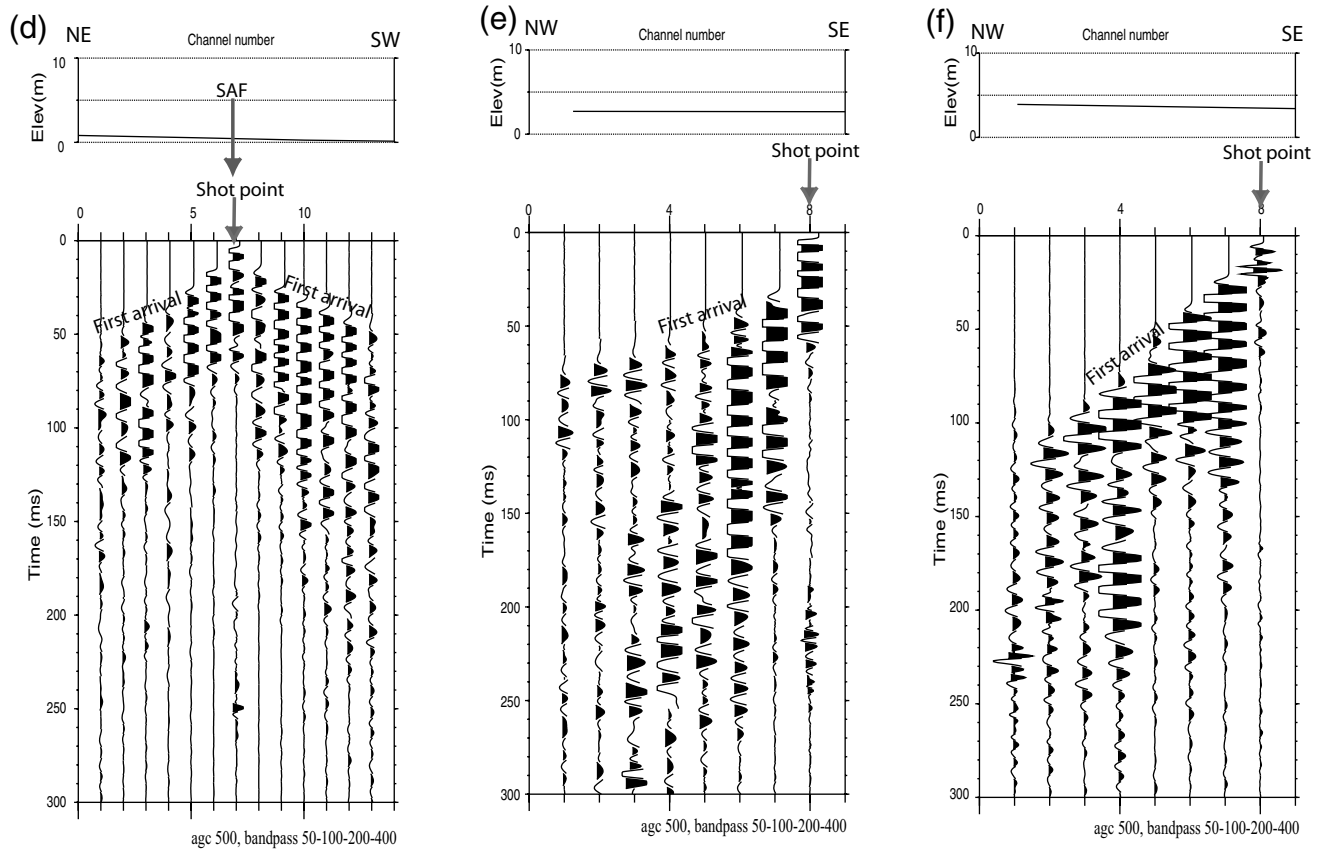

Figure 4. Continued.

be unconsolidated and unsaturated Quaternary alluvial fan deposits. Velocities between about 1500 and 3000 m/sec probably represent compacted or poorly consolidated alluvial deposits that are most likely saturated. Velocities in excess of 4000 m/sec at 24 m in depth probably represent fractured gneiss (Gandhok *et al.*, 1999; Yule *et al.*, 2001). Toward the southwest end of line 1, velocity contours below the 20 m depth dip northeastward between 50 and 65 m. Although the change in structure occurs near the southwest end of line 1, we suggest that this change in velocity represents a major structural change.

Combined Line 1 Refraction/Reflection Image

The combination of seismic velocities and reflection images can be used to aid in interpreting the subsurface structure (Fig. 5). Reflectors with velocities less than 1500 m/sec extend to about 10 m in depth and probably represent unsaturated and unconsolidated alluvial deposits. A change in velocity coincides with a change in the reflection character, whereby the reflectors apparently are more closely spaced. A more irregular reflection pattern occurs from 15 to 20 m in depth, and velocities in that depth range are between about 1500 and 3000 m/sec. From about 15 to about 30 m in depth, we interpret the subsurface to be predominately saturated sediments and fractured rock. The high velocity (>3500 m/sec) suggests that the rocks below the 20 m depth probably represent metamorphic rocks observed in nearby rock outcrops (see Fig. 2b) (Matti *et al.*, 1985; Yule *et al.*, 2001)

Line 2 Reflection Section

Line 2 trends northeast–southwest, parallel to line 1, and it crosses the active surface trace of the SAF (Fig. 3). Migrated seismic reflection images of the upper 100 m along line 2 are shown in Figure 5. Near-surface subhorizontal strata appear to be less than about 10 m thick, and some of the apparent layering may be due to weathering horizons in rock. On the migrated images, most of the strata on the northeastern half of the line are subhorizontal, but strata southwest of 30 m dip southwestward, suggesting that the principal fault zone is centered near 30 m. Individual layers appear to have apparent vertical offsets near the central part of the line at depths of about 20 m, and discontinuous diffractive energy suggests multiple faults. However, due to the poorly layered strata, individual strands of the fault are difficult to identify with certainty on the reflection images.

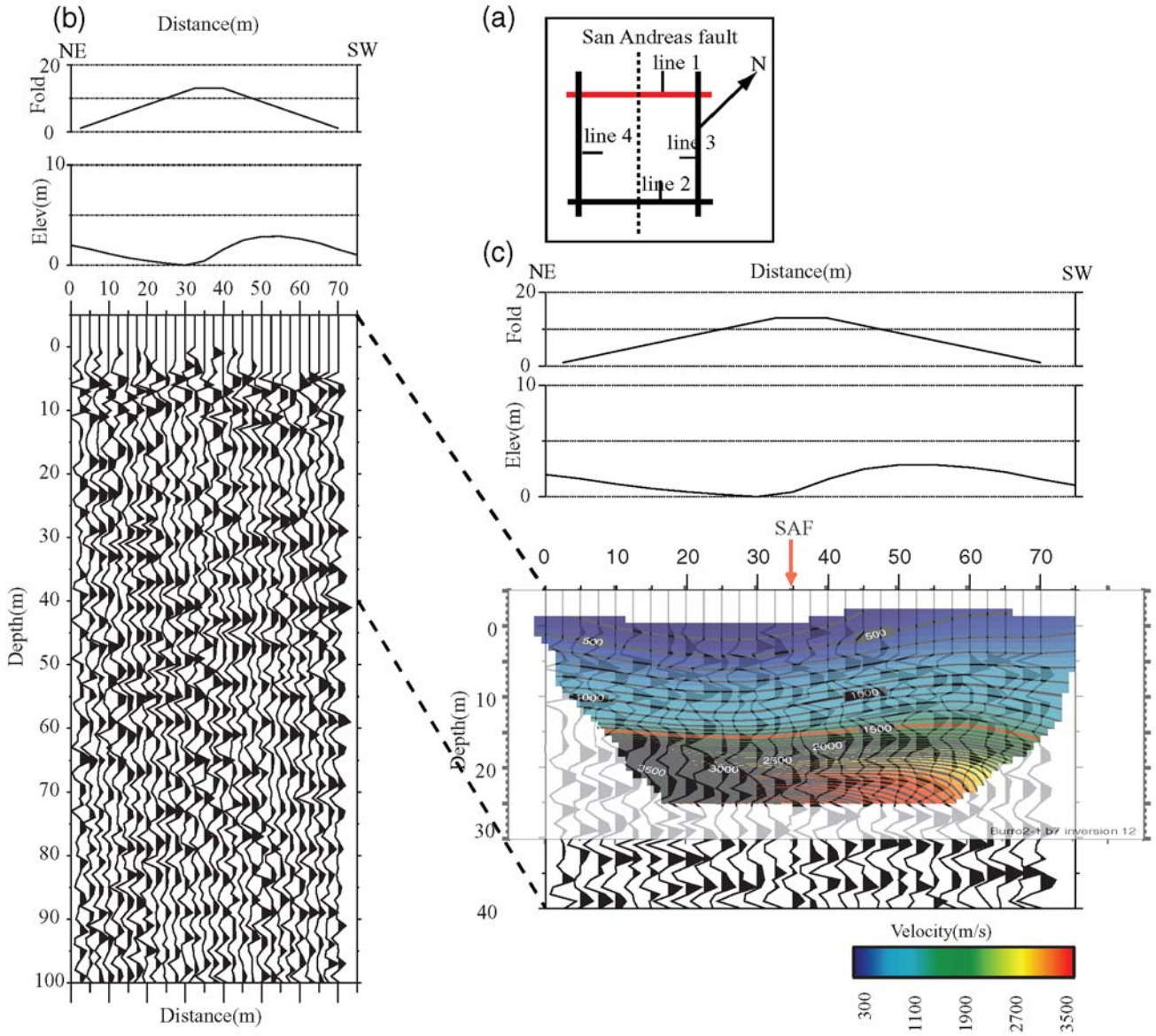

Figure 5. (a) Map showing the setup of the Burro Flats seismic investigation. The red line shows line 1. (b) Migrated seismic reflection image along line 1, with fold and elevation located above the reflection image. (c) Refraction tomography velocity model along line 1 superimposed on the upper 40 m of the migrated reflection image. The fold and elevation is plotted above the combined image. Velocities are shown in meters per second. The surface trace of the San Andreas fault is shown by the red arrow. (d) Map showing the setup of the Burro Flats seismic investigation, with line 2 shown in red. (e) Migrated seismic reflection image along line 2, plotted as in Figure 5b. (f) Refraction tomography velocity model and upper 40 m of the reflection image along line 2, plotted as in Figure 5c. (*Continued*)

Line 2 Refraction Section

P-wave velocities along line 2 range from about 400 to about 6000 m/sec at about 25 m in depth (Fig. 5). Most near-surface (upper 11 m) rocks along line 2 are relatively low in velocity (<1500 m/sec), but near 30 m, there is an abrupt rise in velocity contours, suggesting a major change in structure or composition. On the northeastern end of line 2, measured velocities are limited to the upper 17 m depth, but the available data at the 15 m depth indicate high velocities on both the southern and northern ends of the line and an approximately 10 m wide zone of relatively low velocities near the center of the line. The central zone of low velocities (near 35 m) is located beneath the surface trace of the active strand of the SAF.

Combined Line 2 Refraction/Reflection Image

The superposition of velocity and the reflection data for line 2 also aid in interpreting the surface (Fig. 5). The combined sections suggest that the principal active strand of the SAF zone crosses the seismic line at about 30 m. Holocene

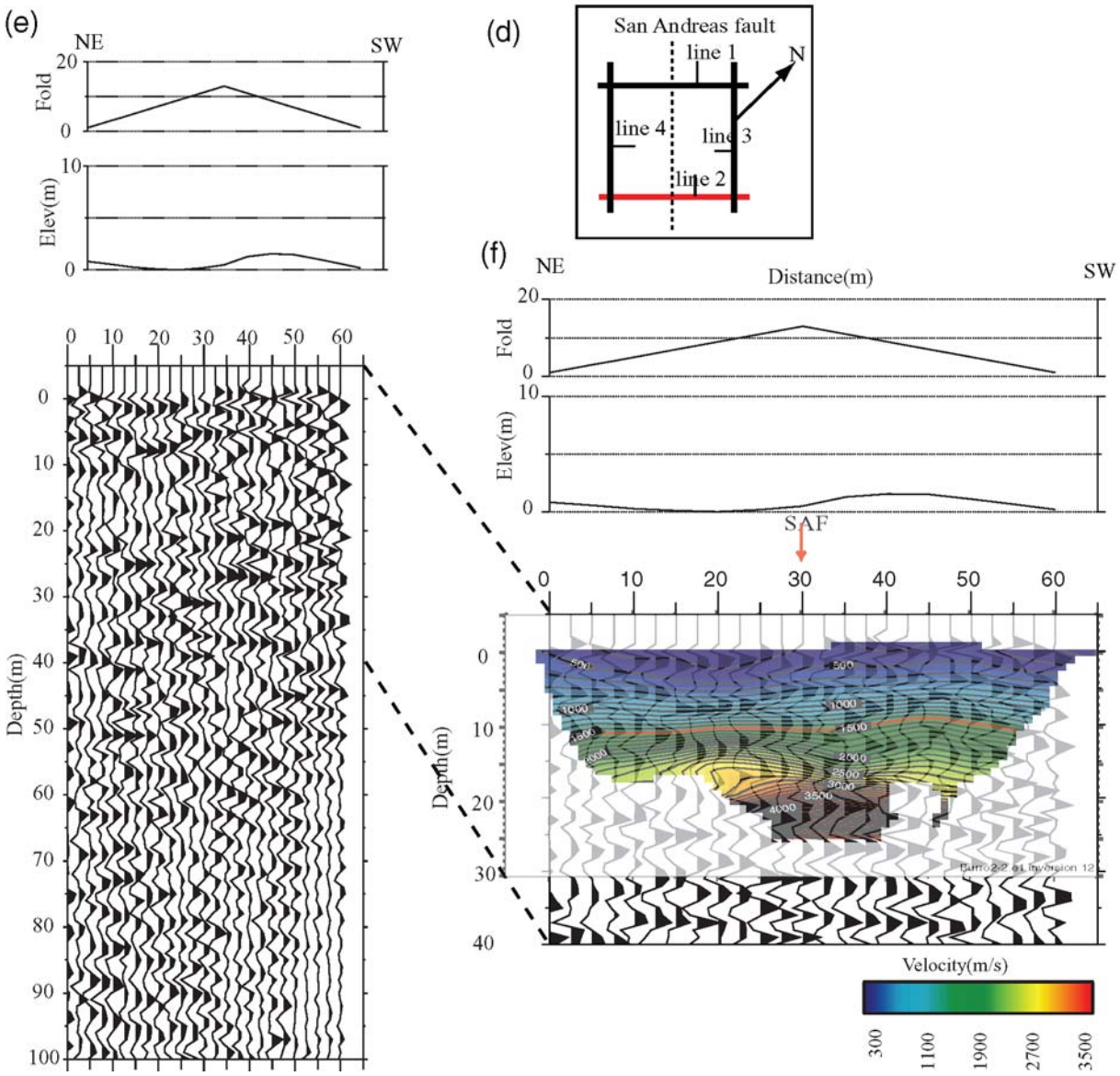

Figure 5. Continued.

alluvial fan deposits, exposed at the surface, coincide with a sequence of thin reflectors with velocities of about 400–1500 m/sec. Reflectors with velocities less than 1500 m/sec likely represent unconsolidated and unsaturated Quaternary sediments. Reflectors below the 23 m depth with high velocities (>5000 m/sec) probably represent Precambrian gneissic rocks.

Line 3 Reflection Section

Line 3 trends northwest–southeast and intersects line 1 on its northwest edge and line 2 on its southeastward edge (Fig. 3). Along line 3, surface rocks consist of Quaternary alluvial and stream deposits. On the basis of near-surface subhorizontal reflections, we interpret these deposits to be less than about 20 m thick, but some of the apparent layering may be due to weathering horizons in the rocks (Fig. 6). At about 45 m of line 3, layers in the upper 30 m dip slightly northwestward. There are principal changes in the reflective character of the seismic section at depths of about 30 m and between 40 and 100 m, which are probably related to differences in lithology.

Line 3 Refraction Section

Seismic velocities ranged from less than 500 m/sec near the surface to more than 3500 m/sec at about 35 m in depth (Fig. 6). There are significant lateral variations in velocity across line 3 in the upper 30 m. Near 10 and 40 m of line 3, there is an abrupt rise of the 700 m/sec *P*-wave velocity

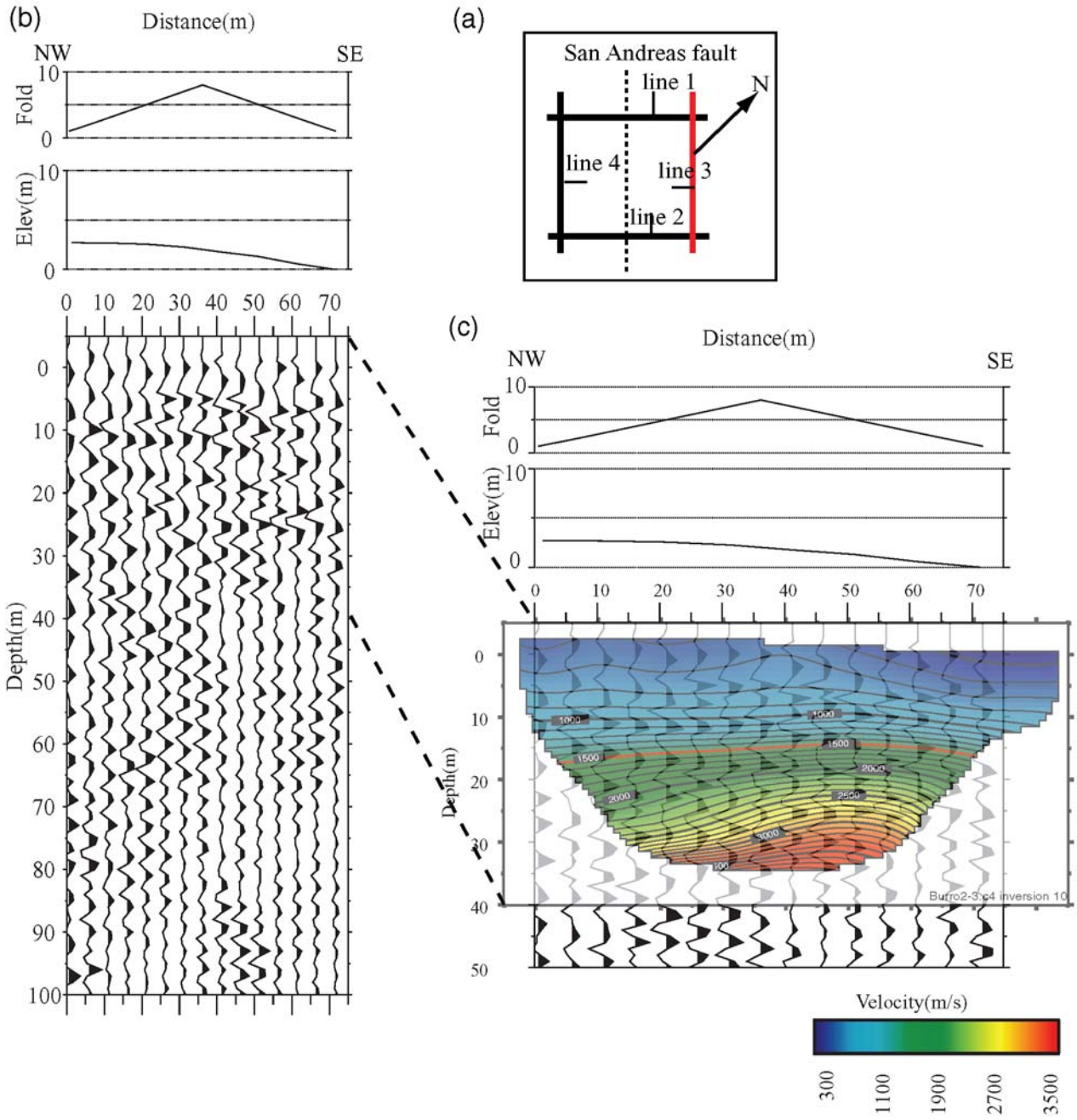

Figure 6. (a) Map showing the setup of the Burro Flats seismic imaging investigation, with line 3 shown in red. (b) Migrated reflection image along line 3, plotted as in Figure 5b. (c) Refraction tomography velocity model and migrated reflection image plotted as in Figure 5c. (d) Map showing the setup of the Burro Flats seismic investigation, with line 4 shown in red. (e) Migrated seismic reflection image along line 4, plotted as in Figure 5b. (f) Refraction tomography velocity model and upper 40 m of the reflection image along line 4, plotted as in Figure 5c. (*Continued*)

contour, but shallow velocities vary considerably. At depths of about 20 m, the highest velocities occur at relatively shallow depths on the southeastern end of the line.

Combined Line 3 Refraction/Reflection Image

The combined section shows that there is a general northwest dip in structure (Fig. 6). Velocities less than about 1500 m/sec extend to depths of about 18 m, and these apparent sediments thicken to the northwest. The underlying rocks with velocities between 3000 and 4000 m/sec probably represent consolidated rock.

Line 4 Reflection Section

Line 4 trends northwest–southeast and intersects with lines 1 and 2 (Fig. 3). Along line 4, we interpret near-surface strata to consist of about 15 m of Holocene alluvial fan

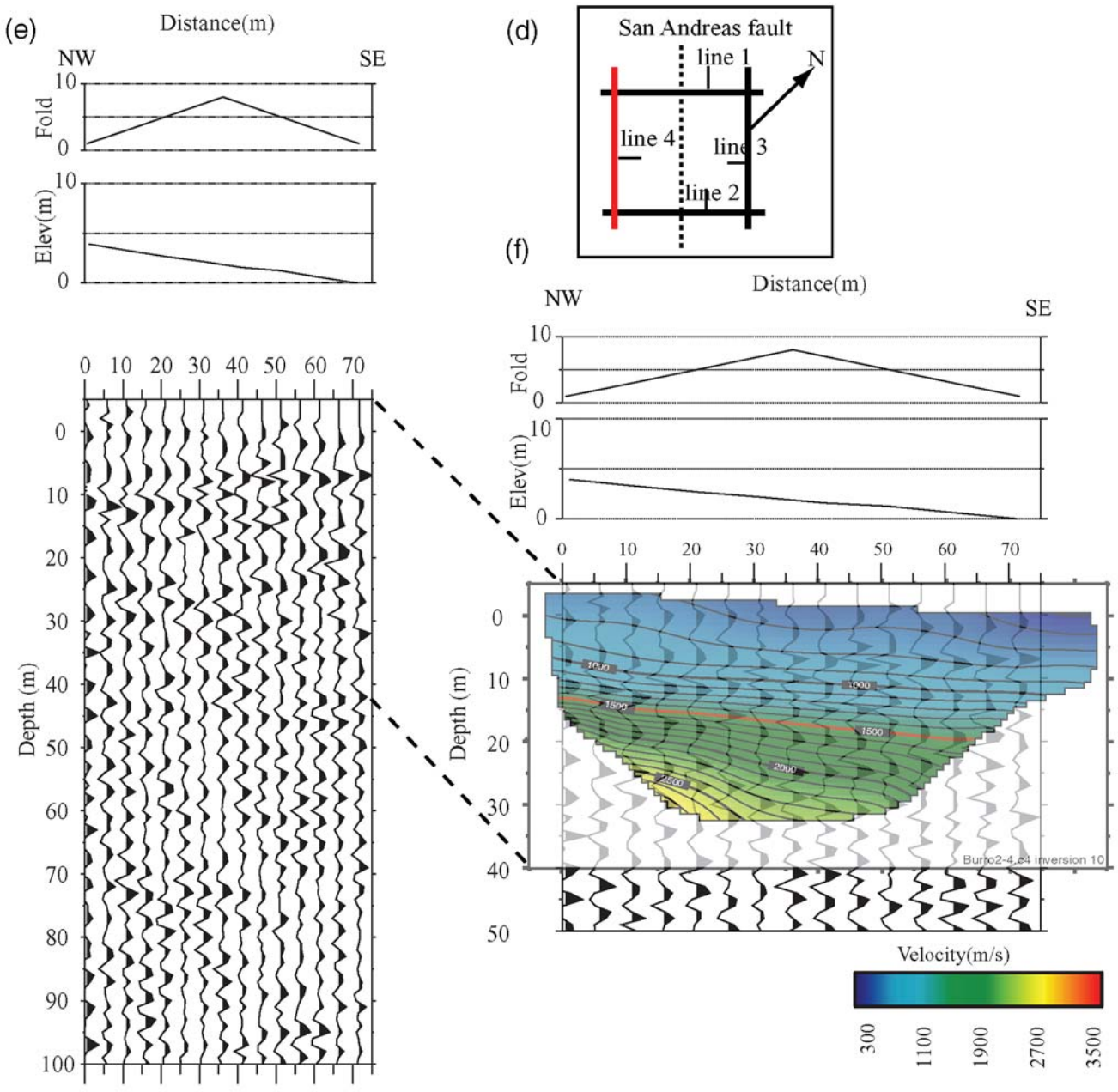

Figure 6. Continued.

deposits; principal changes in reflectivity at about 20 m in depth between 30 and 100 m are likely related to differences in lithology (Fig. 6).

Line 4 Refraction Section

P-wave velocities along line 4 range from about 600 m/sec at the surface to about 2700 m/sec at depths of about 30 m (Fig. 6), with the maximum velocities lower than observed along the other seismic profiles. The highest velocities occur on the northwestward end of line 4. The 2500 m/sec velocity contour dips southeast of 20 m of line 4, suggesting a significant change in rock type below the 25 m depth. Velocities less than 1500 m/sec at depths of about 15 m likely represent unconsolidated and unsaturated Holocene sediments. These sediments appear to be thicker in the southeastern part of the section.

Combined Line 4 Refraction/Reflection Image

A sequence of thin reflectors correlates with velocities less than 1500 m/sec in the upper part of line 4 (Fig. 6). We interpret these low-velocity strata to be up to 20 m of sediments that thicken to the southwest.

Groundwater Depth

Seismic *P*-wave velocities increase significantly in sediments that are greater than 90% of water saturation (Nur, 1982). Such saturated sediments have minimum *P*-wave velocities of about 1500 m/sec (Schon, 1996), and empirical studies in California have shown strong correlations between the depths of groundwater aquifers and the 1500 m/sec velocity contour determined from refraction tomography (Catchings *et al.*, 1998; Gandhok *et al.*, 1999). Some apparent vertical down-on-the-south displacements along the San Bernardino strand of the SAF form groundwater barriers (Bechtel, 1970). We compare the reflection and the refraction data to infer the top of the groundwater table (blue and green lines in Fig. 7). Comparing the water table interpreted from the reflection and velocity images, the 1500 m/sec contour of the velocity model (blue contour) correlates with reflections (green line) from the probable top of the water table (Fig. 7). Along the four lines, minimum depths of the groundwater table, as inferred from the 1500 m/sec velocity contour, range from 10 to about 20 m. The largest variations in depth to the top of the groundwater table occur in areas near mapped faults (Fig. 7), suggesting that groundwater flow in the Burro Flats is strongly affected by the presence of fault strands. Along lines 1 and 2, which cross the surface trace of the SAF, the depth of the 1500 m/sec contour increases from about 10 to 20 m, further suggesting that the fault strands form groundwater barriers. Toward the southeastern end of line 3, the depth of the groundwater table apparently increases slightly, but, along line 4, it appears to decrease to about 20 m. The maximum depth of the groundwater table can be inferred on the basis of the thickness of Quaternary deposits (Catchings *et al.*, 2007). In general, the groundwater table appears to vary little along lines 3 and 4, but it appears to vary appreciably along lines 1 and 2, which cross the surface trace of the SAF.

Imaging of Crustal Faults

Faulting at Burro Flats is known to be highly complex (Yule *et al.*, 2001), and our interpreted faults (Fig. 7) are consistent with the complexities inferred from surface mapping (Yule *et al.*, 2001). We use color variations to highlight differences in the reflection character, with brown coloring delineating a sequence of thin reflectors with close spacing between reflectors. We interpret these reflectors to be unconsolidated alluvial deposits. We used alternating yellow and white coloration to outline sequences of reflectors with wider spacing. On each of the seismic profiles, reflectors above about 10 m probably correspond to Holocene alluvial deposits, and reflectors below about 15 m in depth probably consist of weathered Precambrian gneissic rocks.

Lines 1 and 2 trend largely perpendicular to the SAF, and offset reflectors suggest multiple near-vertical fault strands along much of the section. However, more pronounced faults appear to be located toward the central part of line 1, surfacing near 10, 25, and 55 m (Fig. 7). In the central part of line 2, there appear to be small horst and graben structures, with each horst or graben being less than 15 m wide. At about 30 m, near-vertical apparent offsets of about 5 m in depth coincide with the general location of the surface trace of the SAF. Along lines 3 and 4, there appear to be small offsets near the surface (Fig. 7a), but these vertical offsets may be related to geometrical variations in shot and geophone arrays. However, in other locations, there are apparent offsets in layers that cannot be attributable to geometrical variations in the geophone or shot arrays; we interpret these offsets in reflectors to be faults when multiple layers have similar offsets.

In general, there are multiple lines of evidence for shallow-depth buried faults within the alluvial-covered Burro Flats, including apparent vertically offset reflectors, abrupt lateral variations in seismic velocities, apparent vertical offsets in the inferred water table, and folded near-surface strata. Apparently vertically offset reflectors are observed from reflection images along both lines 1 and 2 (separated by 75 m) in similar geographical locations. Many fault zones have low *P*-wave velocities relative to areas adjacent to the fault zones (Aki and Lee, 1976; Catchings *et al.*, 2002). Along line 2, we observe low-velocity anomalies near the mapped surface traces of the SAF and other apparent faults, which coincide with apparently vertically offset reflectors that had not been previously identified as fault strands. These faults form an apparent flower structure, which is consistent with strike-slip faulting (Harding and Lowell, 1979). The presence of other near-surface fault strands are also indicated by vertical variations in the groundwater table, as many faults are known to act as barriers to groundwater flow, which results in differing depths to the groundwater table on each side of the fault. Because water-saturated sediments typically have *P*-wave velocities of 1500 m/sec or greater (Schon, 1996; Catchings *et al.*, 1999; Gandhok *et al.*, 1999), the 1500 m/sec velocity contour in our tomographic velocity models likely represent variations in the minimum depth of the groundwater table along lines 1 and 2.

Discussion and Conclusion

The shallow-depth velocity structure revealed in this study is useful for understanding the shallow lithology, and it indirectly suggests where low-velocity sediments may amplify during an earthquake. *P*-wave velocities less than 3000 m/sec likely represent unconsolidated sediments and sedimentary rocks at the Burro Flats. Geologic mapping suggests that most of the surface is covered by peat, but a young alluvial fan has built out into the marsh. The most recent alluvial fan deposits have filled the basin and buried the faults. Here, the primary fault that bounds the basin juxtaposes poorly sorted, older, very coarse gravel against interbedded peat, sand, and coarse gravel (Yule *et al.*, 2001). Velocities greater than 3000 m/sec are also difficult to categorize because they may correspond to well-lithified sediments or

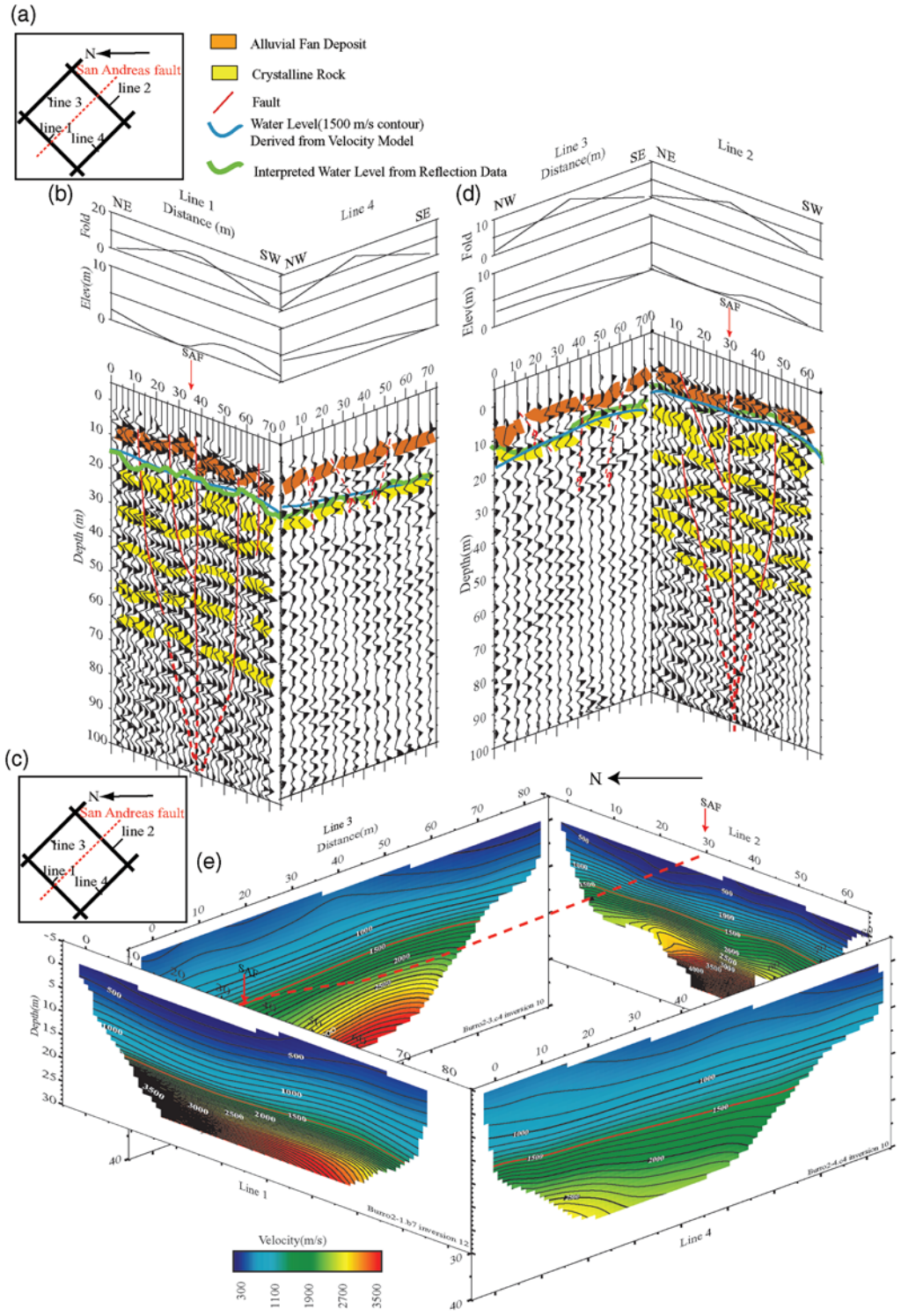

Figure 7. (a) Map showing the setup of the Burro Flats seismic imaging investigation. (b) Migrated seismic reflection images along lines 1 and 4, with reflection horizons highlighted in brown and yellow. Brown colored reflectors correspond to unconsolidated sediments, with velocities less than about 1500 m/sec. The alternating yellow and white reflectors are interpreted as weathering or density layering within the bedrock. Interpreted fault strands that produced apparent vertically offset layers are shown in red. The 1500 m/sec velocity contour (blue) and the coincident interpretative top of the groundwater table (green) are shown superimposed on the reflection image. (c) Map showing the setup of the Burro Flats seismic imaging investigation. (d) Migrated seismic reflection images along lines 2 and 3, plotted as in Figure 7b. (e) Fence diagram of refraction tomography velocity models along lines 1, 2, 3, and 4. Velocities are shown in meters per second. The near-surface location of the San Andreas fault is inferred by the dashed red line. The 1500 m/sec velocity contour is shown in red.

highly fractured crystalline rock. Laboratory studies show crystalline rock and sedimentary rock have *P*-wave velocities in the 3000–3500 m/sec range (Birch, 1960). The observed velocities are consistent with the velocities determined from other high-resolution studies in California. Velocities in excess of 5000 m/sec probably represent crystalline Precambrian gneissic rocks.

Catchings *et al.* (2002) suggest flower structures (Harding and Lowell, 1979) within the low-velocity zones (LVZ) of the SAF at Parkfield, whereby faulted, fractured, and altered rocks with a wide LVZ at shallow depths taper to narrow LVZ at greater depths. From lines 1 and 2, which cross the SAF, the LVZ is most prominent along line 2, below the 10 m depth southwest of and beneath the surface trace of SAF (Fig. 5). At about a 13 m depth, the LVZ is about 10 m wide.

Another issue of importance for studies at Burro Flats is the location of both subsidiary faults and the SAF. At Burro Flats, the SAF consists of a series of right-lateral step-overs and pull-apart basins. Studies of the Burro Flats site suggest that short north-striking faults splay off the main fault zone into the marsh (Yule *et al.*, 2001). Yule *et al.* (2001) interpret these as right-lateral normal oblique faults that transfer slip across the pull-apart basin. This marsh possesses clear evidence of faulting, high sedimentation rates, and a yearly supply of organic material that is critical for obtaining high-precision radiocarbon ages. The marsh, created by a fault acting as a barrier to groundwater, serves as a depocenter for interfingering organic soils and alluvial layers (Yule *et al.*, 2001). We imaged these faults with combined velocity and reflection images, where the upper 20 m is characterized by a sequence of closely spaced thin reflectors (Fig. 7). The stacked seismic reflection images suggest that the most pronounced offsets of stratigraphic layers occur along lines 1 and 2 (Fig. 7). The offset reflections imaged on these two seismic lines, combined with the lateral changes in velocity, indicate that faults extend to the near surface along those seismic profiles, suggesting relatively recent movement on the imaged faults.

The seismic data suggest that the upper 10 m of the subsurface along the seismic lines consist largely of unconsolidated sediments. The groundwater table (1500 m/sec) appears to range from about 10 to 20 m below the ground surface, with a slight decrease in depth along lines 1 and 2 (Fig. 7). There is apparent faulting along most of these lines, but the smaller faults do not appear to affect the depth of the 1500 m/sec contour. Because the velocity model has been laterally and vertically smoothed, the 1500 m/sec contour may not accurately reflect small changes in the depth to water level. If the reflection that correlates with the 1500 m/sec contour results from changes in the depth of the groundwater table, then the reflection image suggests that the groundwater table rises by several meters (to the southwest) across the faults. However, the more prominent faults near the central part of the array suggest that the groundwater table is affected by the presence of faults to a greater extent. The seismic data, both reflection images and velocity images, suggest lateral variation in the subsurface stratigraphic layers. Because lines 1, 2, 3, and 4 intersect, the four lines can be combined into a quasi 3D image of the study area (Fig. 7).

The images show lateral variation in the major lithologic units between the lines. Although some of the individual layers within the upper and lower units are discontinuous across the area of the seismic survey, most layers are continuous across the area. Lines 1 and 2 cross the main surface trace of the SAF, confirming the location of inferred fault trace. Because velocities and gradients are similar in these lines, we suggest that the high-velocity rocks on both sides of the LVZ (and below the surface trace of the SAF) may be similar rock masses that have been dissected locally by the SAF. The lateral extent of the imaged thrust faults is not known, but if the imaged faults are comparable to the mapped thrust faults on both sides of Burro Flat, the imaged faults are probably laterally connected to other thrust faults by high-angle faults. The presence of such faults across most of the Burro Flats within the San Gorgonio Pass suggests that the hazards to the Pass, its infrastructure, and through-going lifelines are greater than those from the fault system located on the northwestern end of the Pass, attested by the large number of seismic events recorded beneath, north, and south of the San Gorgonio Pass between 1981 and 1993 (Magistale and Sanders, 1996). The thick accumulation of low-velocity sediments observed in our seismic survey and that underlie most of the San Gorgonio Pass is likely to amplify shaking induced by the movement on San Andreas and others (e.g., San Jacinto) (Catchings *et al.*, 1999).

In summary, we determined the shallow velocity structure on both sides of the SAF at Burro Flats and identified the main subsurface trace and other fault traces. The location of the fault traces and the amount of offset across a fault can provide an important gauge of the fault movement and thus of earthquake activity, as averaged over multiple earthquake cycles.

Data and Resources

Seismic data from this report are available by contacting R. D. Catchings at the address listed in the author affiliations at the end of the article.

Acknowledgments

We thank Walter Mooney, Gini Gandhok, Ju-Chih Chen, and Char-Shin Liu for providing helpful reviews of an earlier version of the manuscript and for adding further constructive comments for the final version. This project was supported by the U.S. Geological Survey's (USGS) Earthquake Hazards Program.

References

Aki, K., and W. H. K Lee (1976). Determination of three-dimensional velocity anomalies under a seismic array using first *P* arrival times from local earthquakes: 1.A homogeneous initial model, *J. Geophys. Res.* **81,** 4381–4399.

Allen, C. R. (1957). San Andreas fault zone in San Gorgonio Pass, southern California, *Geol. Soc. Am. Bull.* **68,** 319–350.

Bechtel, Incorporated (1970). Water transmission project: engineering feasibility report, appendix A, *Geology*, Consultant Report, San Bernardino Valley Municipal Water District, San Bernardino, California, 41 pp.

Birch, F. (1960). The velocity of compressional waves in rocks to 10 kilobars, part 1, *J. Geophys Res.* **65,** 1083–1103.

Brouwer, J., and K. Helbig (1998). Shallow high-resolution reflection seismics, in K. Helbig and S. Treitel (Editors), *Handbook of Geophysical Exploration: Seismic Exploration*, Vol. **19**, Elsevier, New York, 391 pp.

Catchings, R. D., G. Gandhok, M. R. Goldman, E. Horta, M. J. Rymer, P. Martin, and A. Christensen (1999). Subsurface, high-resolution, seismic images from Cherry Valley, San Bernardino County, California: implications for water resources and earthquake hazards, *U.S. Geol. Surv. Open-File Rept. 99-26*, 57 pp.

Catchings, R. D., M. R. Goldman, W. H. K. Lee, M. J. Rymer, and D. J. Ponti (1998). Thrust faults apparently related to and possible coseismic origin of surface cracks in Potrero Canyon, Los Angeles County, California, following the 1994 Northridge, California, earthquake, *Bull. Seismol. Soc. Am.* **88,** 1379–1391.

Catchings, R. D., M. R. Goldman, C. E. Steedman, G. Gandhok, and M. J. Rymer (2007). Near-surface structure and velocities of the northeastern Santa Cruz Mountains and western Santa Clara Valley from the high-resolution western Santa Clara Seismic Imaging (SCSI) profile, *U.S. Geol. Surv. Open-File Rept. 07-1039*.

Catchings, R. D., M. J. Rymer, M. R. Goldman, J. A. Hole, R. Huggins, and C. Lippus (2002). High-resolution seismic velocities and shallow structure of the San Andreas fault zone at Middle Mountain, Parkfield, California, *Bull. Seismol. Soc. Am.* **92,** 2493–2503.

Fraser, D. M. (1931). Geology of the San Jacinto quadrangle south of San Gorgonio Pass, *Calif. Div. Mines 27th Rept. of State Mineralogist*, 494–540.

Fumal, T. E., M. J. Rymer, and G. G. Seitz (2002). Timing of large earthquakes since A.D. 800 on the Mission Creek strand of the San Andreas fault zone at Thousand Palms Oasis, near Palm Springs, California, *Bull. Seismol. Soc. Am.* **92,** 2841–2860.

Gandhok, G., R. D. Catchings, M. R. Goldman, E. Horta, M. J. Rymer, P. Martin, and A. Christensen (1999). High-resolution seismic reflection/refraction imaging from Interstate 10 to Cherry Valley Boulevard, Cherry Valley, Riverside County, California: implications for water resources and earthquake hazards, *U.S. Geol. Surv. Open-File Rept. 99-320*, 52 pp.

Harding, T. P., and J. P. Lowell (1979). Structural styles, their plate tectonic habitats, and hydrocarbon traps in petroleum provinces, *Am. Assoc. Pet. Geol. Bull.* **63,** 1016–1058.

Hole, J. A. (1992). Nonlinear high-resolution three-dimensional seismic traveltime tomography, *J. Geophys. Res.* **97,** 6553–6562.

Jones, L., K. Hutton, D. Given, and R. C. Allen (1986). The North Palm Springs, California, earthquake sequence of July 1986, *Bull. Seismol. Soc. Am.* **76,** 1830–1837.

Magistrale, H. M., and C. Sanders (1996). Evidence from precise earthquake hypocenters for segmentation of the San Andreas fault in San Gorgonio Pass, *J. Geophys. Res.* **101,** 3031–3044.

Matti, J. C., and D. M. Morton (1993). Paleogeographic evolution of the San Andreas fault in southern California: a reconstruction based on a new cross-fault correlation, in *The San Andreas Fault System: Displacement, Palinspastic Reconstruction, and Geologic Evolution*, R. E. Powell, R. J. Weldon II and J. C. Matti (Editors), *Mem. Geol. Soc. Am.*, **178,** 107–159.

Matti, J. C., D. M. Morton, and B. F. Cox (1985). Distribution and geologic relations of fault systems in the vicinity of the Central Transverse Ranges, southern California, *U.S. Geol. Surv. Open-File Rept. 85-365*.

Nicholson, C. (1996). Seismic behavior of the southern San Andreas fault zone in the northern Coachella Valley, California: comparison of the 1948 and 1986 earthquake sequences, *Bull. Seismol. Soc. Am.* **86,** 1331–1349.

Nur, A. (1982). Notes on wave propagation in porous rocks, *Stanford Rock Physics Progress Report, January 1982*, Vol. **13**, Stanford University, Stanford, California, 121 pp.

Rymer, M. J. (2000). Triggered surface slips in the Coachella Valley area associated with the 1992 Joshua Tree and Landers, California, earthquakes, *Bull. Seismol. Soc. Am.* **90,** 832–848.

Schon, J. H. (1996). Physical properties of rocks: fundamentals and principals of petrophysics, in *Handbook of Geophysical Exploration 18* K. Helbig and S. Treitel (Editors), Pergamon Press, Elsevier Science, Inc. New York, 583 pp.

Sharp, R. V., M. J. Rymer, and D. M. Morton (1986). Trace-fractures on the Banning fault created in association with the 1986 North Palm Springs earthquake, *Bull. Seismol. Soc. Am.* **76,** 1838–1843.

Yule, D., and K. Sieh (2001). The paleoseismic record at Burro Flats: evidence for a 300-year average recurrence for large earthquakes on the San Andreas fault in San Gorgonio Pass, southern California (abstract), *Geol. Soc. Am. Abstr. Prog.* **33,** no. 3, 31.

Yule, D., and K. Sieh (2003). Complexities of the San Andreas fault near San Gorgonio Pass: implications for large earthquakes, *J. Geophys. Res.* **108,** 2548, doi 10.1029/2001JB000451.

Yule, D., T. Fumal, S. McGill, and G. Seitz (2001). Active tectonics and paleoseismic record of the San Andreas fault, Wrightwood to Indio: working toward a forecast for the next "big event", in *Geologic Excursions in the California Deserts and Adjacent Transverse Ranges*, Geological Society of America Cordilleran Section and American Association of Petroleum Geologist, Pacific Section, Society for Sedimentary Geology Pacific Section, Fullerton, California, 91–126.

U.S. Geological Survey
345 Middlefield Road
MS 977
Menlo Park, California 94025
(C.C.T., R.D.C., M.R.G., M.J.R.)

Institute of Oceanography
National Taiwan University
P.O. Box 23-13
Taipei, Taiwan 106
(P.S.)

Institute of Geophysics
National Central University
Jhongli, Taoyuan 32001
Taiwan
(H.W.C.)

Manuscript received 8 December 2006